the FEBS Journal

From steady-state to synchronized yeast glycolytic oscillations I: model construction

Franco B. du Preez[1], David D. van Niekerk[2], Bob Kooi[3], Johann M. Rohwer[2] and Jacky L. Snoep[1,2,3]

1 Manchester Institute of Biotechnology, The University of Manchester, Manchester, UK
2 Triple J Group for Molecular Cell Physiology, Department of Biochemistry, Stellenbosch University, Matieland, South Africa
3 Theoretical Biology and Molecular Cell Physiology groups, Vrije Universiteit, Amsterdam, The Netherlands

Keywords
glycolysis; limit-cycle oscillation; mathematical model; model construction; *Saccharomyces cerevisiae*

Correspondence
J. L. Snoep, Triple J Group for Molecular Cell Physiology, Department of Biochemistry, Stellenbosch University, Private Bag X1, Matieland 7602, South Africa
Fax: +27 218085863
Tel: +27 218085844
E-mail: jls@sun.ac.za

(Received 19 January 2012, revised 5 June 2012, accepted 12 June 2012)

doi:10.1111/j.1742-4658.2012.08665.x

An existing detailed kinetic model for the steady-state behavior of yeast glycolysis was tested for its ability to simulate dynamic behavior. Using a small subset of experimental data, the original model was adapted by adjusting its parameter values in three optimization steps. Only small adaptations to the original model were required for realistic simulation of experimental data for limit-cycle oscillations. The greatest changes were required for parameter values for the phosphofructokinase reaction. The importance of ATP for the oscillatory mechanism and NAD(H) for inter-and intra-cellular communications and synchronization was evident in the optimization steps and simulation experiments. In an accompanying paper [du Preez F *et al*. (2012) *FEBS J* doi:10.1111/j.1742-4658.2012.08658.x], we validate the model for a wide variety of experiments on oscillatory yeast cells. The results are important for re-use of detailed kinetic models in modular modeling approaches and for approaches such as that used in the Silicon Cell initiative.

Database
The mathematical models described here have been submitted to the JWS Online Cellular Systems Modelling Database and can be accessed at http://jjj.biochem.sun.ac.za/database/dupreez/index.html.

Introduction

Two different approaches are generally used in systems biology studies for construction of kinetic models: a so-called 'top-down' approach, which is largely data-driven and used for describing experimental data for large networks (up to genome scale), and a 'bottom-up' approach with more mechanistic, biochemical techniques that is used for smaller systems, typically at the pathway level [1]. Ultimately, combinations of the two approaches may enable kinetic descriptions of large systems, whereby the level of detail at which the system is described gradually increases as bottom-up models replace top-down models [2,3].

Bottom-up models require detailed kinetic information at the reaction level. Typically this is enzyme kinetic data, measured under physiological conditions. Although it would appear to make good sense to re-use such models, this has not traditionally been the approach. Often models are created to address a specific research question, and, depending on how the models were constructed, they may have only little usability for other studies. On the other hand, if the parameters used in a kinetic model were experimentally determined, it is not immediately clear why they cannot be re-used in other models, and their values should not be changed if a model is merged with another

Abbreviations
F16P, fructose-1,6-bisphosphate; GAPDH, D-glyceraldehyde-3-phosphate dehydrogenase; PFK, 6-phosphofructokinase.

model (as in modular modeling approaches). Importantly, parameters for such models should be determined under physiological conditions, i.e. conditions that reflect the conditions in which the enzymes are active *in vivo*. This approach is more fully described in the Silicon Cell initiative [4].

Re-usability is dependent on the accessibility of models and standardization of model descriptions. Ideally, data and models are annotated (e.g. MIRIAM [5]), curated, and stored in standard formats (e.g. SBML [6]), schematically represented in SBGN format [7], and made available through publication of scientific studies in curated model repositories such as Biomodels [8], JWS Online [9], DOCQS [10] and CellML [11]. With the advent of large systems biology projects, important progress has been made in data and model management. One such data and model management system is SEEK [12], which is used in a number of large European systems biology projects.

In this paper, we test the re-usability of a classic bottom-up model for one of the best studied metabolic pathways, the yeast glycolytic model, which has been described in [13] and is referred to here as the Teusink model. This model has been used in several other studies, e.g. to investigate the control patterns of yeast glycolysis over a large range of enzyme activities [14], to investigate the effects of transcript regulation on glycolytic enzymes in response to varying oxygen concentrations [15], and to study the influence of harvesting cells at the diauxic shift on steady-state behavior [16].

In addition to the Teusink model constructed by the Amsterdam group, a large number of other kinetic models for yeast glycolysis have been published [17–24], all of which followed a different approach for model construction, either fitting parameters on system behavior, or using simplified core models.

For the Teusink model, the authors tested whether *in vivo* system behavior can be predicted by a model constructed purely on the basis of experimentally measured *in vitro* enzyme kinetic parameters [13]. The model was validated for a specific steady state: anaerobic glucose fermentation under non-growing conditions. Here we test whether it is possible to adapt the model to describe a qualitatively different behavior: glycolytic oscillations.

Oscillatory behavior of yeast glycolysis has been observed in cell extracts and in intact cells, and can be induced under specific experimental conditions: harvesting cells at the diauxic shift, starvation for glucose and subsequent addition of glucose and cyanide. The oscillating concentrations of the majority of glycolytic intermediates have been followed experimentally in yeast cultures [25] and extracts [26]. Spectroscopy of NADH is routinely used to determine characteristic behaviors of the intact pathway, of which synchronization of oscillations in yeast populations is probably one of the most intriguing. Two out-of-phase oscillating yeast populations rapidly synchronize their oscillations upon mixing, and acetaldehyde has been proposed as the communicating agent between the cells [27,28].

Mathematical models describing glycolytic oscillations were originally highly abstracted [29,30], and were used to study the mechanism of oscillations. Such core models have also been used more recently [19] to study higher-level behavior, such as synchronization and changes in the oscillation frequency in response to the concentration of external glucose. The kinetic parameters in these models do not have a direct mechanistic interpretation, and are often assigned values for which the behavior of interest emerges. A disadvantage of such core model-based approaches is that high-level behaviors such as strong synchronization cannot be related back to the individual reactions of the pathway. More recently, models of increasing detail that describe glycolytic oscillation in yeast have been published [18,22,24]. The Teusink model has also been used previously to describe glycolytic oscillations [31], but in that case local changes to glucose transport, ATP-consuming processes and branches of glycolysis were used to obtain a model for which the limit cycle did not closely resemble existing experimental data for the oscillations. Thus far the kinetic model described previously [18] is the most detailed model, with a realistic description of the glycolytic oscillations. However, all of these models (core and detailed) were fitted to a specific data set or type of behavior, and used to test hypotheses or just to test whether the model can describe the data; there was little or no validation of the constructed models.

Here we focus on the following question: can we simulate the experimentally observed oscillations within small ranges of the original parameter set of the Teusink model? To address this question, we used a small experimental data set to train the model. We have tried to stay close to the original (experimentally measured) parameter values, and have used local optimization methods. The aim was not to perform a full calibration of the parameters but to only adjust the parameters that strongly improve the model behavior with respect to its comparison with the training data set. In an accompanying paper, we validate the model by testing its predictive power for a wide range of experimental data sets, without further calibration of the model parameters [32]. The model was able to predict the observed behavior at least qualitatively, and in

some cases quantitatively, using a single parameter set for the enzyme kinetic rate equations, and using external parameter values close to the experimental conditions (e.g. biomass concentrations, external metabolite concentrations, flow rates). This is an important finding for the field of computational systems biology as it indicates that detailed mechanistic models may be used for quantitative descriptions of qualitatively different behavior.

The mathematical models described here have been submitted to the JWS Online Cellular Systems Modelling Database and can be accessed at http://jjj.biochem.sun.ac.za/database/dupreez/index.html. The models dupreez1 to 4 are available in SBML format and can be simulated at http://jjj.biochem.sun.ac.za/.

Results

Adaptations to the original steady-state model

The Teusink model [13] was originally constructed to describe one specific steady-state condition. The authors focused on the main glycolytic pathway, and chose to include fixed fluxes for the trehalose and glycogen synthesis branches with values equal to the measured fluxes for the experimental conditions. In addition, they incorporated simple kinetics for the ATPase reaction and the succinate and glycerol branches. These fixed flux values and simple kinetics were sufficient to describe the specific steady state under which Teusink *et al.* performed their experiments, but severely limit the flexibility of the model and restrict its usage for different conditions. To extend the range of conditions under which the Teusink model can be used, we replaced the fixed flux values for the trehalose and glycogen synthesis branches with simple irreversible mass action kinetics, yielding identical fluxes at steady state. The adenylate kinase reaction, which was assumed to be in equilibrium in the Teusink model, was simulated using rapid mass-action kinetics, as we did not want to impose an equilibrium constraint on the reaction under the highly dynamic conditions. We also chose to represent ATP, ADP and AMP explicitly, instead of using a variable for the energy-rich phosphate bonds, P, as used in the original model ($P = 2 \times \mathrm{ATP} + 1 \times \mathrm{ADP}$), and the general ATPase reaction was changed from linear to saturation kinetics. We included more kinetic detail in the glycerol branch by modeling the intermediate glycerol-3-phosphate and its dephosphorylation [20]. Note that all these changes were applied in such a way that the original steady state as described by the Teusink model was not altered in the adapted model (changes $< 1.4\%$, see Table 1), and that only reactions for which no detailed kinetic information was available in the Teusink model were altered. The reaction network

Table 1. Comparison of the steady-state flux and metabolite levels for the adjusted model, dupreez1 (column I) and the original Teusink model [13] (column II). The following reactions were changed in the dupreez1 model: glycogen and trehalose synthase, adenylate kinase and glycerol 3-phosphate dehydrogenase. The kinetics for these reactions were chosen such that the steady state of the original model was not affected (changes < 1.4%). Glyoxylate shunt equals the succinate production in the Teusink model. For definition of abbreviations, please see Fig. 1.

	Flux (mM·min^{-1})			Concentration (mM)	
Reaction	I	II	Metabolite	I	II
GLT	88.10	88.08	Glucose	0.09945	0.09985
GLK	88.10	88.08	G6P	1.019	1.010
Glycogen synthase	6.019	6.000	F6P	0.1103	0.1087
Trehalose synthase	2.408	2.400	F16P	0.5980	0.5973
PGI	77.26	77.28	Triose phosphates	0.7747	0.7741
PFK	77.26	77.28	1,3-BPG	0.0003228	0.0003200
Aldolase	77.26	77.28	P3G	0.3540	0.3533
G3PDH	18.19	18.20	P2G	0.04448	0.04437
GAPDH	136.3	136.4	PEP	0.07255	0.07216
PGK	136.3	136.4	Pyruvate	8.500	8.502
PGM	136.3	136.4	Acetaldehyde	0.1700	0.1701
Enolase	136.3	136.4	ATP	2.510	2.504
Pyruvate kinase	136.3	136.4	ADP	1.315	1.323
PDC	136.3	136.4	AMP	0.3098	0.3144
ADH	129.1	129.1	NAD	1.561	1.563
Glyoxylate shunt	3.637	3.641	NADH	0.04489	0.04488
			ATPase	84.34	84.39

for the adapted model, referred to as dupreez1, and all the models derived from it are shown in Fig. 1.

Obtaining an oscillating model

The original Teusink model [13] is formulated in terms of ordinary differential equations, which describe the change in metabolite concentrations as a function of the enzyme kinetic rate equations. We used the same formulation of ordinary differential equations for our model descriptions. In a first step to simulate the oscillatory behavior, we focused on the stability of the steady state in the Teusink model. The stability of a steady state is characterized by the time-dependent behavior of variables upon perturbation of the steady state; if the variable moves back to the steady state, it is called stable, and if the variable moves away from the steady state, it is called unstable.

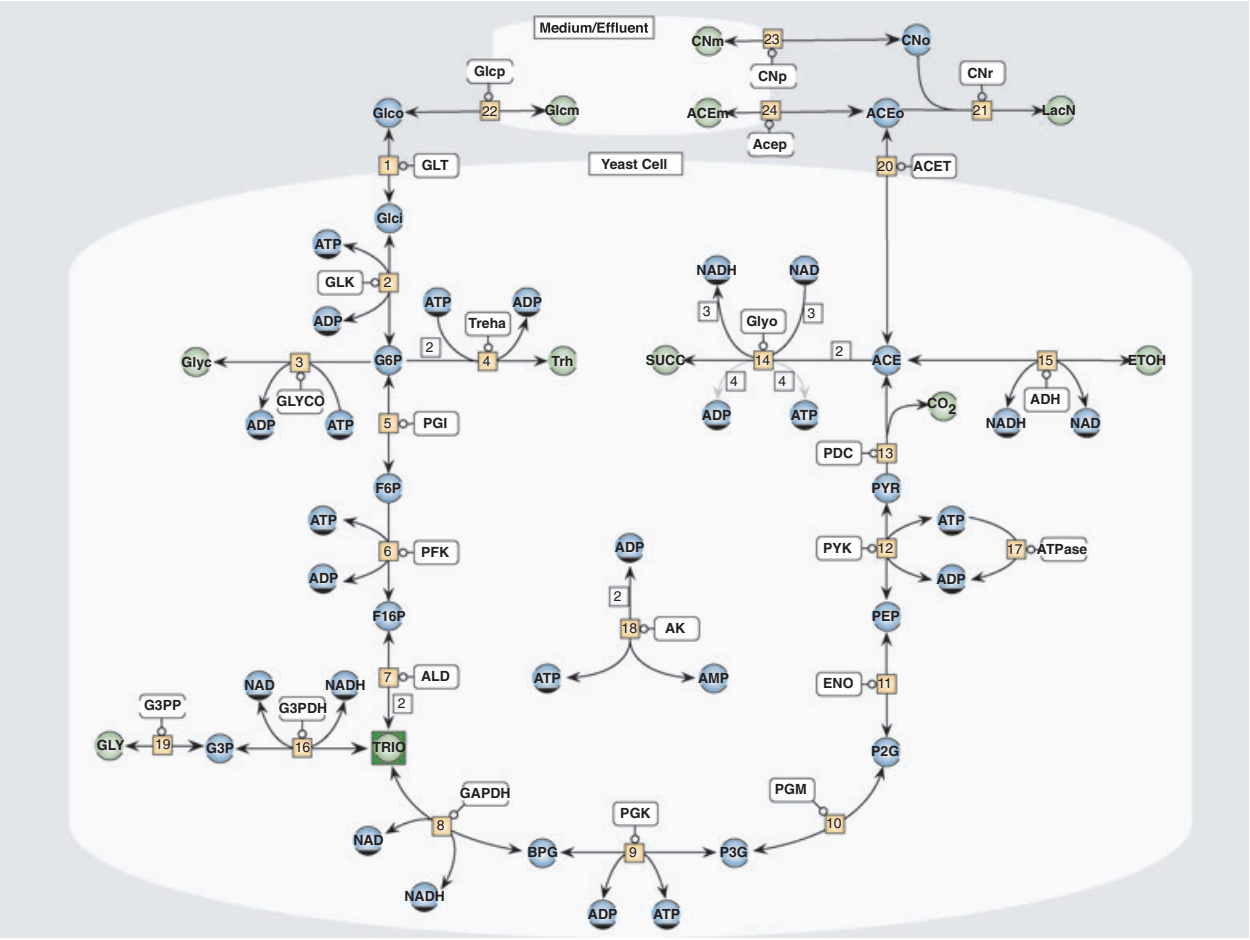

Fig. 1. Reaction network for the glycolytic models. The original Teusink model consists of reactions 1–18, including glucose transport, glycolysis, and the branch reactions to trehalose, glycogen and succinate. In the Teusink model reactions 16 and 19 were combined as a single reaction for glycerol production, and reaction 18 was modeled as an equilibrium block. The reaction network for the models dupreez 1 to 3 consists of reactions 1–19. Reactions 20 and 21, acetaldehyde transport and complex formation with cyanide were added for model dupreez4, to include cell-cell interactions, necessary for the synchronization studies. ACE, acetaldehyde; ADH, alcohol dehydrogenase (EC 1.1.1.1); AK, adenylate kinase (EC 2.7.4.3); ALD, fructose-1,6-bisphosphate aldolase (EC 4.1.2.13); BPG, 1,3-bis-phosphoglycerate; ENO, phosphopyruvate hydratase (EC 4.2.1.11); F16P, fructose-1,6-bisphosphate; F6P, fructose 6-phosphate; GAP, D-glyceraldehyde-3-phosphate; GAPDH, D-glyceraldehyde-3-phosphate dehydrogenase (phosphorylating) (EC 1.2.1.12); G3P, glycerol 3-phosphate; G3PDH, glycerol 3-phosphate dehydrogenase (EC 1.1.99.5); G6P, glucose 6-phosphate; GLYCO, glycogen branch; HK, hexokinase (EC 2.7.1.1); P2G, 2-phosphoglycerate; P3G, 3-phosphoglycerate; PEP, phosphoenolpyruvate; PDC, pyruvate decarboxylase (EC 4.1.1.1); PGI, glucose-6-phosphate isomerase (EC 5.3.1.9); PFK, 6-phosphofructokinase (EC 2.7.1.11); PGK, phosphoglycerate kinase (EC 2.7.2.3); PGM, phosphoglycerate mutase (EC 5.4.2.1); PYK, pyruvate kinase (EC 2.7.1.40); PYR, pyruvate; TPI, triose phosphate isomerase (EC 5.3.1.1); Tps1, trehalose 6-phosphate synthase (EC 2.4.1.15); TREHA, trehalose branch; SUC, succinate branch.

The sensitivity of the reaction rate (v) for variable changes, ($\frac{\partial v}{\partial S}$), is given by the Jacobian matrix (M); specifically at the steady-state concentrations of the (independent) metabolites (S°), M_{S°:

$$M_{S^\circ} = N \cdot \left.\frac{\partial \nu}{\partial S}\right|_{S=S^\circ} \quad (1)$$

where N is the stoichiometric matrix, which is used to express the ordinary differential equations in terms of rate equations. The response to a small perturbation of the steady state (ΔS) is described by:

$$\frac{d\Delta S}{dt} = M_{S^\circ} \cdot \Delta S \quad (2)$$

The eigenvalues and eigenvectors of M_{S° can be used to describe the changes in ΔS in the linearized model. For a steady state to be stable, the real parts of all eigenvalues must be negative, as was the case for the original Teusink model [13] and our modified model (dupreez1). Generally, for reaction networks where all processes are product-inhibited and substrate-activated, there are no destabilizing values in M_{S°, and, after perturbation, all variables will relax monotonously to their steady-state values. Product activation or substrate inhibition, whether direct or indirect, stoichiometric or kinetic, is a prerequisite for non-monotonous dynamic behavior but not necessarily a sufficient condition to generate sustained oscillations. The eigenvalues of the Jacobian matrix for our modified model (dupreez1) and for the original model [13] contained one complex conjugate pair. Such a non-zero imaginary component affects the dynamics with which a variable relaxes after perturbation, but the real part of the eigenvalue determines the stability of the steady state. When the real part of an eigenvalue of the Jacobian matrix passes through zero, the system becomes unstable; the point where this occurs is called a Hopf bifurcation. For oscillatory behavior to arise, a system has to move through the Hopf bifurcation; it will then have eigenvalues with a positive real component and also non-zero imaginary components (complex conjugate pair).

To obtain oscillatory behavior for the dupreez1 model, we used an algorithm based on the eigenvalues of the Jacobian matrix to search for a Hopf bifurcation. The objective function that the algorithm maximizes is the ratio of the absolute values of the imaginary to real parts of the conjugate pair (referred to as the Hopf objective). Control of a rate on this ratio indicates to what extent a particular reaction will affect the oscillatory tendency of the model. We have defined coefficients analogous to those commonly used in metabolic control analysis [33,34]:

$$C^{\frac{Im\,\lambda_j}{Re\,\lambda_j}}_{\nu_i} = \frac{\partial \ln\left|\frac{Im\,\lambda_j}{Re\,\lambda_j}\right|}{\partial \ln \nu_i} \quad (3)$$

where λ_j represents either of the eigenvalues in the conjugate pair.

In a first optimization step, we used a gradient descent algorithm to increase the oscillatory tendency of the model (as defined in the Hopf objective) by adjusting the activities of individual enzymes according to the value of their control coefficients as defined in Eqn (3). At the Hopf bifurcation point, the Hopf objective reaches a maximum value, and our first optimization algorithm, which is based on Eqn (3) without additional cost functions, searches for such a point.

The steepest descent search yielded a set of V_{max} values for which the real part of the complex conjugate pair of eigenvalues passed through zero, and where the model (referred to as the dupreez2 model) exhibited limit-cycle oscillations at a frequency of 3.34 min^{-1}, with a supercritical Hopf bifurcation for external glucose concentrations. Note that the Hopf objective is generic; it is not limited to a specific model. We have used the same objective for a number of steady-state models that have the potential to oscillate, and we obtained oscillatory conditions for each of these models (data not shown).

The adjustments to the original V_{max} values resulting from our optimization procedure are listed in Table 2 (dupreez2 model). Although many of the V_{max} values were changed during this first optimization routine, we noted high control coefficients on the oscillatory behaviour for three enzymes in particular: glucose transport, glyceraldehyde-3-phosphate dehydrogenase (GAPDH) and ATPase.

Mean concentration and largest amplitude

The first optimization step brought our model close to a supercritical Hopf bifurcation point, leading to limit-cycle oscillations with a small amplitude. To move the model beyond the bifurcation point, we used the fructose 1,6-bisphosphate amplitude (which is the largest amplitude) and the mean concentrations of the other metabolites [25] as the data set for model fitting. We used a gradient descent method guided by the sum of normalized squared differences. Initially we allowed only for changes in the concentration of enzymes, to simulate changes in the expression level of the enzymes during the glucose starvation used in preparation of the cells for oscillation experiments, but found no set of V_{max} values that could describe the large amplitude

Table 2. V_{max} values for the four models. Absolute values are given for the dupreez1 model, and are very close to the values in the original Teusink model. Values for the other models, dupreez2, 3 and 4 are given relative to the value in dupreez1 (as percentages). Units for V_{max} values in dupreez1 are (mM·min^{-1}), except for glycogen synthase and AK (mM^{-1}·min^{-1}), trehalose synthase (mM^{-2}·min^{-1}), and the glyoxylate shunt (min^{-1}). For definition of abbreviations, please see Fig. 1.

	Model			
Enzyme	dupreez1	dupreez2	dupreez3	dupreez4
GLT	97.264	140	65.2	45.2
GLK	226.452	146	126	101
Glycogen synthase	2.35413	71.8	41.5	27.9
Trehalose synthase	0.941652	80.1	53.2	37.7
PGI	339.677	138	92.9	80.8
PFK	182.903	100	74.8	69.7
Aldolase	322.258	72.3	46.6	35.9
G3PDH	477.424	100	5.28	4.16
G3PA	538.371	101	6.69	5.34
GAPDH	1184.52	35.4	27.4	23.6
PGK	1306.45	109	78.8	61.1
PGM	2525.81	109	79.5	63.0
Enolase	365.806	126	95.8	75.5
Pyruvate kinase	1088.71	161	122	112
PDC	174.194	129	97.1	120
ADH	810	103	59.3	40.7
Glyoxylate shunt	21.4	91.6	78.0	72.5
ATPase	93.1853	73.8	45.1	41.1
AK	133.333	100	72.1	90.9

of fructose-1,6-bisphosphate (F16P) as observed experimentally.

When we extended the optimization to include more kinetic parameters (excluding equilibrium constants and external variables), this allowed for a significant decrease in the objective function and a much better description of the experimental data set. Although the mean concentration of NADH was included in the objective function, it was not adjusted sufficiently in the optimization procedure. For a better fit to the mean NADH concentration, we ran a second round of optimization specifically to increase the mean NADH concentration. The frequency of the oscillations after this second optimization step was 2.02 min^{-1}. We adjusted the frequency of the model to the experimentally measured frequency (1.45 min^{-1}) by adjusting all V_{max} values by a factor of 1.45/2.02. We refer to the resulting model as dupreez3. We have listed the enzyme activity changes for this model relative to the activities in the dupreez1 model in Table 2, and the changes to other kinetic constants are listed in Table S2. The greatest kinetic changes were to 6-phosphofructokinase (PFK), but none of the parameter values were adjusted by more than a factor of 1.4 or smaller than 0.6 times the original values in dupreez1.

In Fig. 2, we compare the limit-cycle oscillation for dupreez3 with the experimental data [25]. As, with exception of the amplitude for F16P, none of the phases and amplitudes were fitted in Fig. 2, the goodness of fit is striking.

Synchronization

For correct description of cell–cell communication via acetaldehyde, which has been shown to be essential for synchronization of oscillations in yeast populations [27, 28], some additional changes to the structure of the Teusink model were required (see Fig. 1, dupreez4 model). In the original Teusink model, no acetaldehyde transport was included, and we adapted the model to allow for this, using rapid mass-action kinetics (see below). Furthermore, addition of a clearance rate for acetaldehyde was required to simulate cyanide addition under the experimental conditions.

The synchronization of oscillations was simulated in models consisting of two cells. The initial metabolite concentrations for each cell were sampled from the trajectory of a limit-cycle oscillation, and were chosen such that the two cells were phase-separated by a specific angle at $t = 0$. During optimization for the synchronization, we varied the phase separation between 1 and 179°. An important factor in simulating the synchronization between cells is the biomass concentration, which is included in the model as the intra- to extracellular volume ratio. For the optimization, we used a volume ratio of 50 : 1 (extracellular to intracellular volume), which is typical for such experiments [18]. We also used the rate constant for acetaldehyde removal by cyanide determined previously [28], setting the cyanide concentration to 5 mM.

Acetaldehyde transport

For acetaldehyde transport across the cell membrane, we assumed passive diffusion using a modified form of Fick's law, which is dependent on the permeability coefficient of the membrane (P), the area of the membrane (A), and the concentration difference across the membrane ($ACA_e - ACA_i$). For the change in internal acetaldehyde concentration:

$$\frac{dACA_i}{dt} = \frac{A \cdot P}{V_i}(ACA_e - ACA_i), \quad (4)$$

the permeability coefficient is dependent on the partition coefficient (K), the diffusion coefficient of

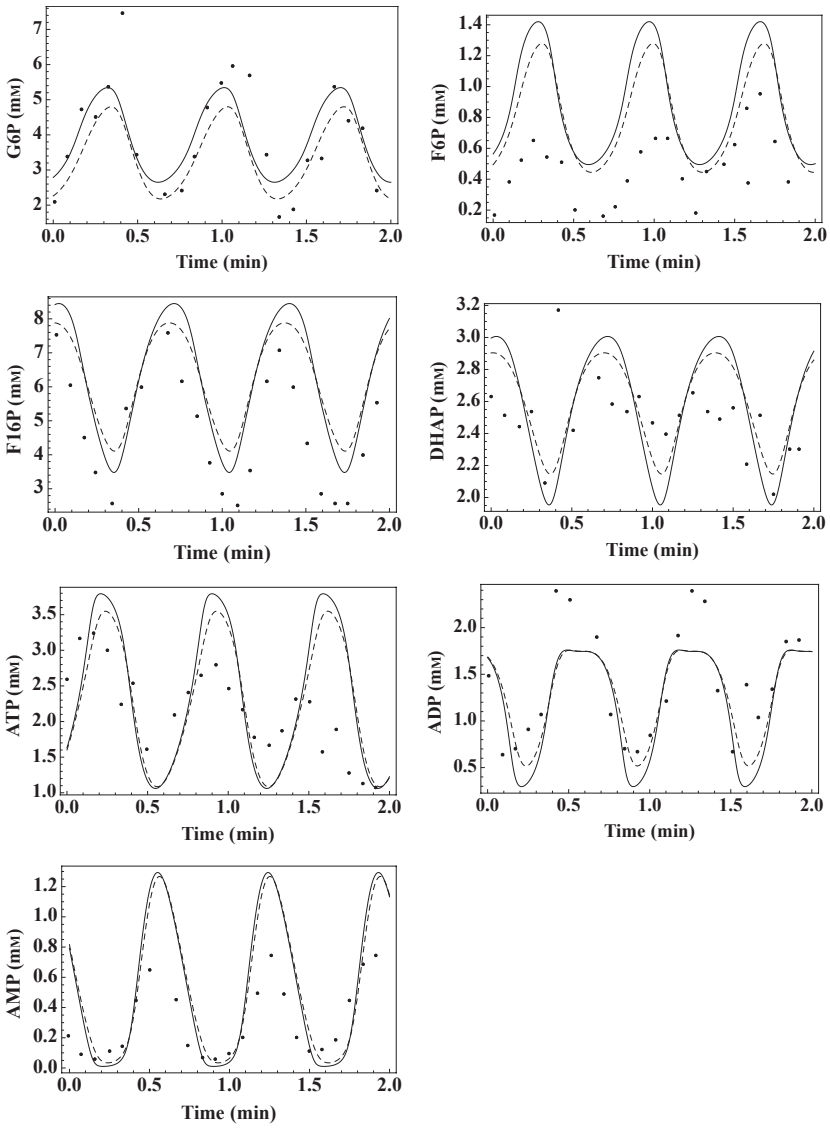

Fig. 2. Comparison of model simulations (dupreez3 and dupreez4) for metabolite concentrations with experimental data [25]. Lines represent model predictions: solid lines for dupreez3 and dashed lines for dupreez4. Experimental data are shown as black dots. For definition of abbreviations see Fig. 1.

acetaldehyde in the membrane (D), and the membrane thickness (x):

$$P = \frac{DK}{x} \tag{5}$$

We could not obtain an experimentally determined value for the permeability coefficient of acetaldehyde (P_{ACA}) from the literature. However, it is possible to calculate P_{ACA} from the permeability coefficient of ethanol (P_{EtOH}) given the partition coefficients for both molecules and assuming that they have equal diffusion coefficients in the cell membrane. We obtained an estimate of 3×10^{-4} cm·s^{-1} for P_{EtOH} [35] measured across the cell membrane of *Saccharomyces cerevisiae*. For the values of the partition coefficients, we used the water/octanol partition coefficients as proxies for cell membrane partition coefficients, with values of 2.7 for acetaldehyde [36] and 0.51 for ethanol [37]. The ratio K_{ACA}/K_{EtOH} equates to 5.3, yielding a value of 1.59×10^{-3} cm·s^{-1} for P_{ACA}. For calculation of the cell volume (V), and surface area (A), we assumed a sphere with a radius of 2 μm, leading to:

$$\frac{\mathrm{dACA_i}}{\mathrm{d}t} = 1431 \cdot (\mathrm{ACA_e} - \mathrm{ACA_i})$$

The value for the transport coefficient of 1431 min^{-1} is significantly higher than that used in the models described previously [18,38], but in a more recent paper, the acetaldehyde transport step over the membrane was assumed to be in equilibrium, i.e. have a much higher value [39]. In these papers, no detailed explanation for the parameter values was given, making it hard to compare the values.

Synchronization objective

Using the dupreez3 model to simulate the interaction of two 180° phase-separated cells, which is similar to the mixing experiment described previously [27,28], resulted in anti-phase synchronization. To improve the synchronization in the model, we included a third optimization step. For this optimization, we quantified the strength of synchronization over a given period T, using the integral of the product of metabolite concentration changes in the two cells (in this case ATP). We used the integration in Eqn (6) as an objective function to guide a gradient descent search for parameters affecting the synchronization tendency of the two-cell model:

$$\int_0^T \left(\frac{\partial \mathrm{ATP}_{\mathrm{cell1}}(t)}{\partial t} \cdot \frac{\partial \mathrm{ATP}_{\mathrm{cell2}}(t)}{\partial t} \right) \mathrm{d}t \qquad (6)$$

When two cells are oscillating with roughly the same phase, the slopes of their metabolite concentrations will have the same sign for the most part, and the product of these slopes will therefore have a positive value. For anti-synchronizing cells, this product will be negative by similar reasoning. By integration of this product of slopes, the synchronization tendency over a time period of interest can be calculated, and this typically consists of initial dynamics plus relaxation to a stable synchronizing or anti-synchronizing state. This can best be visualized by plotting this integral as a function of the integration window (T). During the optimization procedure for maximal synchronization, T was chosen to capture the pronounced growth or decay of the initial phase shift; during the optimization, Eqn (6) becomes linear with time, with a positive slope for synchronizing cells and with a negative slope for anti-synchronizing cells (see Fig. S1).

Synchronization results

We first applied this algorithm at low extracellular to intracellular volume ratios and at a low phase separation between the cells. The algorithm was then re-run several times with increasing volume ratios and phase separations. This yielded a parameter set for which two cells synchronize up to 180° phase separation (dupreez4 model) (see Fig. 1 for the reaction network, Table 2 for the $V_{\max}$ values, and Table S2 for all parameter values). Interestingly, the enzyme activities showing the largest responses were linked directly to the nicotinamide moieties (alcohol dehydrogenase, glycerol and succinate production), which have been previously implicated in synchronization of individual cells [38]. Reactions producing NADH increased the synchronization tendency (succinate production), while those producing NAD^+ decreased it (glycerol and alcohol dehydrogenase). The rate of synchronization was slower than, but comparable to, that seen experimentally, as it takes between 20 and 30 cycles for the model to synchronize, compared to 10 cycles in mixing experiments (Fig. 3).

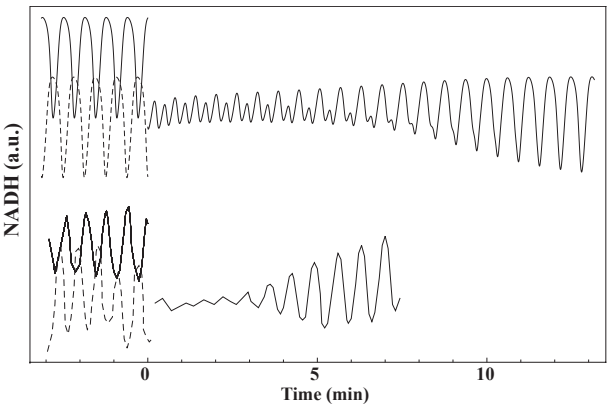

Fig. 3. Synchronization of out-of-phase oscillations. Simulations for two out-of-phase yeast cells (top; dupreez4 model for two cells with 170° phase separation) and experimental data for out-of-phase yeast populations (bottom [28]) are shown before mixing from $t = -3$ to 0 min, and after mixing at $t = 0$. The two cultures (or cells in the simulation) are shown separately before mixing (as dashed and solid lines), and as a mean signal after mixing. The y axis has arbitrary units.

Discussion

In consecutive steps, three objective functions were optimized in order to adapt an existing detailed kinetic model for the steady-state behavior of yeast glycolysis to simulate oscillatory behavior. The original model parameters were adapted (most parameters were changed by $< 20\%$) by fitting the model to a small subset of available experimental data.

There have been numerous developments in recent years in terms of experimental design and parameter estimation for systems biology; these have been summarized in a recent mini-review series [40–42]. In the first of these reviews, Ashyraliyev *et al.* [40] define identifiability of parameters in terms of their unique determination given a certain profile of input data and the resultant parameter estimation. Factors such as correlation of parameters contribute to lack of identifiability. The authors summarize various approaches to search parameter space, including global and local optimization methods. Cedersund and Roll [41] discuss the question of how to compare and assess two or more competing explanations (models) for a given set of experimental

data, perhaps incorporating prior knowledge. They focus on residual analysis as a method to reject a particular model, and introduce statistical tests such as the Akaike information criterion, which calculates in-sample error, to compare two or more models. Importantly, they not only compare different parametrizations of the same model but address the question of comparing models with different structures. In the final review, Kreutz and Timmer [42] focus on optimal experimental design in terms of a combination of experimental stimulations and observations, in order to estimate parameters by optimization and to discriminate between models. Using the statistics of experimental design, they show how to eliminate interfering factors and co-variates. For optimization, various cost functions based on the Fisher information matrix (i.e. the inverse of the covariance matrix of the estimated parameters) are presented.

It should be emphasized that all the approaches reviewed in the mini-review series address the question of discriminating between alternative models for explaining the same data set, or identifying model parameters by model optimization against experimental observations. This was not the approach in the present paper; instead, we started out from a given model with identified parameters, and determined whether the same model can reproduce dynamic behavior that is completely different from the conditions under which it was originally built, and to what extent it must be modified to achieve this.

Our approach is close to that taken previously [18], where the authors started with a detailed kinetic model constructed on the basis of enzyme kinetic data from the literature. The authors did not allow changes to the enzyme kinetic rate equations or the kinetic parameters taken from the literature; they fitted the so-called 'velocity parameters' (V_{max} values for the reactions) using a 'direct method'. The direct method uses stationary data at the Hopf bifurcation in an optimization procedure that is not dependent on integration of the ordinary differential equations, i.e. it is direct because it can use algebraic equations. Using this method with a limited parameter set allowed the authors to perform a more global search for optimal parameter values. However, the authors were only able to use stationary data for their optimization method, and although they were able to extract important information concerning the dynamics of the oscillatory signal from the Jacobian matrix at the Hopf bifurcation point, this limits their data set to this reference point.

In contrast to the direct method, we used a more explicit formulation of an objective function, optimization of which involves integration of the ordinary differential equations. This less efficient method (i.e. much more computer-intensive), in addition to inclusion of a larger parameter set, limited us to the use of a local parameter optimization method. In addition, we had to rely on a sequential optimization procedure, as combined optimization of all three objectives was not workable and computationally too intensive. An advantage of the explicit formulation is that it does not limit us to information that is directly related to the Hopf bifurcation; for instance, we were able to include the generic information that the cells synchronize in our third optimization step.

We started our approach by adjusting the V_{max} values for the enzyme kinetic rate equations in an existing model for yeast glycolysis [13]. Some of the V_{max} values had to be adjusted significantly more than what may be attributed to experimental error. It should be realized that the original model was based on experimental data for compressed yeast (Koningsgist from DSM Bakery Ingredients, Heerlen, The Netherlands), while most of the oscillation studies were performed using a different *S. cerevisiae* strain, X2180. The physiological state of compressed yeast may be comparable to the state of cells harvested at the diauxic shift (as is done for oscillation experiments), but it is to be expected that inter-strain differences would lead to significant changes in kinetic parameters. In addition, in oscillation experiments, cells are starved of glucose for 2 h, and this may result in significant changes in enzyme expression levels.

The effects of glucose starvation on fermentative capacity, and V_{max} measurements before and after 24 h starvation have been reported [16, 43]. Although most of the starvation effects appeared to be strain-specific, a strong decrease (to 50% of the activity before starvation) was measured for the glucose transport step in both studies, and a significant increase in alcohol dehydrogenase activity was also reported. Most of the other enzymes were not significantly affected: PFK was up-regulated in one study [16] but down-regulated in the other [43], significant increases in fructose-1,6-bisphosphate aldolase and phosphoglycerate kinase activity were reported in one study [43] but not the other [16], and phosphopyruvate hydratase was significantly down-regulated in one study [43] but not the other [16]. Except for the 50% decrease in glucose transport activity, which is very similar to the adaptation made in our final model (55% decrease in dupreez4), there was no good correlation between the adaptations made in our optimization steps and the reported changes during 24 h glucose starvation.

Analyzing the adjustments that were made to the V_{max} values, it is clear that most of the values were

reduced compared to the original V_{max} values, specifically after adjustment of the enzyme activities to fit the oscillation frequency (Table 2). Although the adjustments may appear to be large (the mean adjustment in dupreez4 is to 56.4% of the original value), it should be noted that the oscillation experiments are performed at a significantly lower temperature (20–25 °C) than applied in the Teusink study (30 °C). Assuming a Q10 value of 2 (i.e. a 10 °C decrease in temperature leads to 1/2 the activity), this temperature difference would result in up to 50% lower enzyme activities for the experimental conditions used by Richard *et al.* [25] compared to the conditions used by Teusink *et al.* [13], and this adjustment is close to what was applied in the model.

In addition to an overall decrease, some specific changes needed to be made in V_{max} values, notably for glyceraldehyde-3-phosphate dehydrogenase, which was the enzyme that was adjusted most after the first optimization step (dupreez2). In fact, we were able to induce limit-cycle oscillations in the dupreez1 model by modification of two enzymes only: reducing the V_{max} of GAPDH and ATPase to 15% and 7% of their activity, respectively, in dupreez1 leads to oscillations (data not shown). The role of GAPDH in shifting the model closer to the Hopf bifurcation may be understood by a closer look at the PFK kinetics, specifically the role of F16P.

Substrate inhibition of PFK (negative allosteric regulation by ATP) is considered to be the key instability that gives rise to glycolytic oscillations [18, 26, 29]. The range of concentrations at which this inhibitory effect is strong is limited to high concentrations of ATP, but a high concentration of F16P extends this concentration range. In the original steady-state model [13], the F16P concentration is low (0.6 mM), and this translates into a small range of adenylate charges inhibiting PFK (Fig. 4A). Down-regulating GAPDH results in an increase of F16P, and this increases the range of substrate concentrations for which high adenylate charges inhibit the system (Fig. 4B).

This first optimization step, in which we limited the parameter set to the V_{max} values of the reaction steps, and used a generic objective function to find the Hopf bifurcation based on a ratio of the imaginary over the real part of the eigenvalue of the Jacobian matrix, is comparable to a method used previously [18]. Similarly to the result obtained previously [18], the Hopf bifurcation in our model is a supercritical Hopf bifurcation, and the amplitude of the oscillation close to the Hopf bifurcation is very small. The optimization criterion for the Hynne model [18] is based on Hopf bifurcation data, and their model shows a much smaller amplitude than observed experimentally.

In a second optimization step, we used the F16P amplitude and mean concentrations of the other metabolites measured previously [25] to pull the model through the Hopf bifurcation to obtain larger amplitudes. In addition to V_{max} values, we had to make changes to other kinetic parameters for this second optimization step to be successful. In dupreez3 and dupreez4, most parameters have a smaller than 20% deviation from the original values (dupreez1) but seven parameters required greater adjustment (Table S2). Strikingly, of these seven parameters, five are from the PFK rate equation. Upon analyzing the effects of the parameter changes on the PFK kinetics, it becomes clear that the ATP inhibition effect that was already enhanced in dupreez2 (Fig. 4B) compared to the original model, was even stronger in dupreez3, to the extent that the large oscillations in ATP concentration, $1.5 < ATP < 2.7$, reported previously [25] can be accommodated. In Fig. 4, we have also shown how the limit-cycle oscillations for ATP are positioned on the

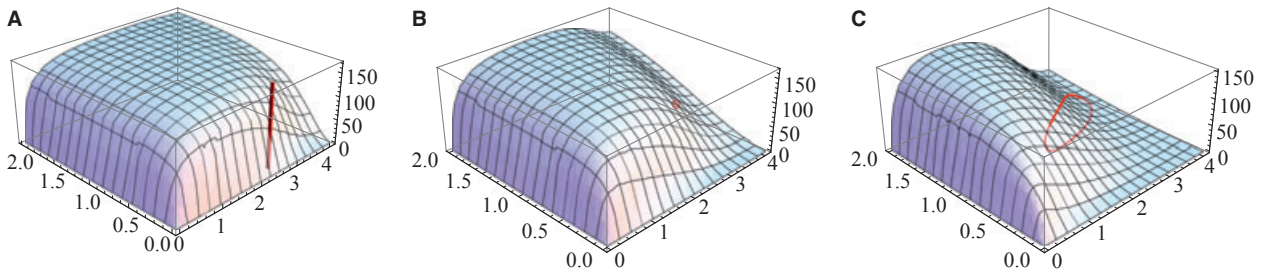

Fig. 4. Comparison of the kinetics for PFK. (A) Original steady-state model (dupreez1, F16P = 0.60 mM). (B) The initial oscillating version (dupreez2, mean F16P = 6.5 mM). (C) after fitting to the F16P amplitude (dupreez3, mean F16P = 4.8 mM). The *x* axis represents ATP (mM), the *y* axis represents the F6P concentration (mM) and the *z* axis represents the reaction rate (mM·min^{-1}). The steady-state concentrations of F6P and ATP is indicated in graph (A) with a bar in (B) and (C), the oscillatory trajectory for F6P and ATP is shown. When ATP was varied, corresponding changes in ADP and AMP were made such that the total pool of adenylates remained constant (for these calculations, adenylate kinase was assumed to be in equilibrium).

contour plot, and it is clear that the oscillatory trajectory of ATP lies in the area of the changed PFK kinetics (Fig. 4B,C).

The extracellular to intracellular volume ratio is a crucial parameter for synchronization of oscillations: increasing the ratio strongly reduces the synchronization tendency [38]. In our model, an experimental volume ratio of 50 : 1, oscillation of two 170° phase-separated cells was synchronized at a somewhat slower rate (within 30 cycles), but was in the same order of magnitude as that seen in mixing experiments (within 10 cycles). We examined the changes to the kinetic parameters that led to fast synchronization. Interestingly, all prominent changes were related to the nicotinamide moieties, causing an increase in the $NADH/NAD^+$ ratio. The presence of cyanide was also found to strongly control the efflux of acetaldehyde, which contributes to the redox strain (increased $NADH/NAD^+$ ratio) necessary for synchronizing individual cells in the model. Our results therefore show that, with the adjustments that increase the $NADH/NAD^+$ ratio, our model predicts strong synchronization at intracellular to extracellular volume ratios typical used in experiments. This result also highlights a role for cyanide in addition to keeping the extracellular acetaldehyde in an optimal concentration range as suggested previously [28], i.e. to create the necessary intracellular redox strain to allow intercellular communication [44].

We used a sequential optimization approach, formulating three objective functions that are optimized in succession. This approach worked well for our specific problem but is not generally robust. Clearly optimization of one objective function may be in conflict with that of another objective function. The approach worked for several reasons. The first objective function is generic and was used to find the Hopf bifurcation, i.e. the onset of oscillatory conditions. The second and third optimization steps only work for oscillatory conditions, so will not violate the first objective. In principle, there may be a conflict between the second and third optimization steps, but it appeared that the most important parameters were not conflicting for the two objectives. Thus, after the third optimization step, the objective for the second optimization step was only slightly reduced, and when one compares the description of data from Richard *et al.* [25] (criterion for the second optimization step) for models dupreez3 and dupreez4, the difference is very small (Fig. 2).

To discuss sequential application of the second and third objectives, we created a bar graph showing the response coefficients for each objective for each reaction (Fig. 5), in which the contribution of the parameters for each reaction at the start of the optimization procedure is indicated. To match the real F16P amplitude and the mean concentrations, as defined in the second objective, changes to the kinetic parameters of the PFK enzyme had by far the most prominent effects (Fig. 5A). In contrast, the optimization to find a synchronizing model (Fig. 5B) showed more distributed responses for the various parameters: in addition to being strongly affected by the parameters of the PFK reaction, the reactions affecting the NADH/NAD ratio were predominant, including alcohol dehydrogenase, glycerol 3-phosphate dehydrogenase and GAPDH, as well as the phosphoglycerate kinase reaction. The latter links oscillations in NADH/NAD to ATP/ADP/AMP, and is thought to communicate synchronization of cells from the extracellular messenger (acetaldehyde) to the PFK reaction, which is important for generating the oscillations [24].

To conclude, using relatively small changes to the enzyme kinetic parameters, it was possible to adapt the Teusink model [13], constructed for simulation of a specific steady state, to describe limit-cycle oscillations and fast intercellular synchronization. Importantly, for adaptation of the model, we only used a small subset

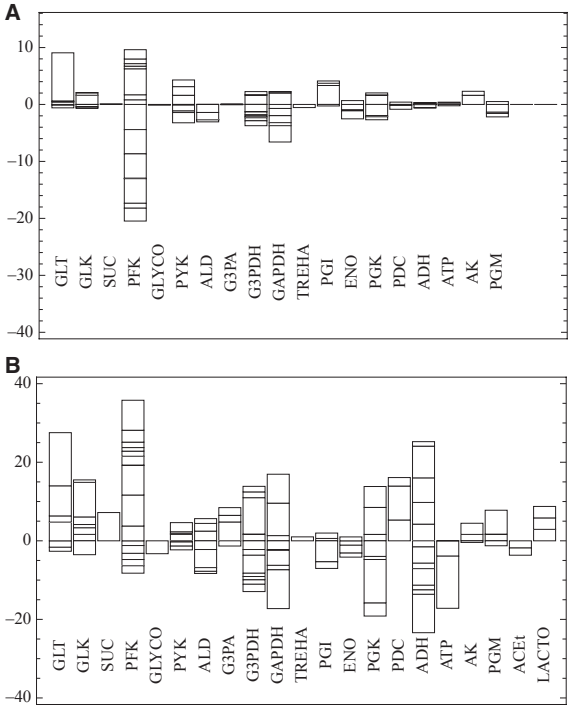

Fig. 5. Response coefficients for the second and third optimization steps. The response coefficients of each of the parameters (stacked in the individual bars) for the objective functions are listed per reaction. (A) Response coefficients for the objective fitting the mean concentration of glycolytic intermediates and F16P amplitude; (B) response coefficients for the synchronization objective. For definition of abbreviations, please see Fig. 1.

of experimental data, and the model was able to describe the observed oscillations reasonably well. In an accompanying paper, we validate the model much more strictly by testing its ability to predict a wide set of independent dynamic experiments [32].

Experimental procedures

Mathematica 8 (Wolfram Research Inc., Champaign, IL, USA) was used for all calculations and simulations. Model simulations were performed using the NDSolve function. The objective functions for the optimization steps were: Eqn (3) for optimization step 1, a normalized sum of squared differences for optimization step 2 [see Eqn (7), with m_i model data and d_i experimental data], and Eqn (6) for optimization step 3:

$$\sum_{i=1}^{n} \frac{(m_i - d_i)^2}{d_i} \tag{7}$$

The specific algorithm for optimization of the objective functions was a self-coded implementation of a steepest decent method, where response coefficients [e.g. Eqn (3)] were used for adjustments of the parameter values.

Acknowledgements

We acknowledge the financial assistance of the UK Biotechnology and Biological Sciences Research Council to F.dP. and J.L.S. via a SysMO-DB grant, and from the National Research Foundation in South Africa to D.D.vN., J.M.R. and J.L.S.

References

1 Westerhoff HV & Palsson BO (2004) The evolution of molecular biology into systems biology. *Nat Biotechnol* **22**, 1249–1252.
2 Snoep JL, Bruggeman F, Olivier BG & Westerhoff HV (2006) Towards building the silicon cell: a modular approach. *Biosystems* **83**, 207–216.
3 Madsen M, Danø S & Quistorff B (2012) A strategy for development of realistic mathematical models of whole-body metabolism. *Open J Appl Sci* **2**, 11–27.
4 Snoep JL (2005) The Silicon Cell initiative: working towards a detailed kinetic description at the cellular level. *Curr Opin Biotechnol* **16**, 336–343.
5 Le Novère N, Finney A, Hucka M, Bhalla U, Campagne F, Collado-Vides J, Crampin EJ, Halstead M, Klipp E, Mendes P *et al.* (2005) Minimum information requested in the annotation of biochemical models (MIRIAM). *Nat Biotechnol* **23**, 1509–1515.
6 Hucka M, Finney A, Sauro HM, Bolouri H, Doyle JC, and the rest of the SBML Forum (2003) The systems biology markup language (SBML): a medium for representation and exchange of biochemical network models. *Bioinformatics* **19**, 524–531.
7 Le Novère N, Hucka M, Mi H, Moodie S, Schreiber F, Sorokin A, Demir E, Wegner K, Aladjem MI, Wimalaratne SM *et al.* (2009) The systems biology graphical notation. *Nat Biotechnol* **27**, 735–741. Erratum in *Nat Biotechnol* **27**, 864.
8 Li C, Donizelli M, Rodriguez N, Dharuri H, Endler L, Chelliah V, Li L, He E, Henry A, Stefan MI *et al.* (2011) Biomodels database: an enhanced, curated and annotated resource for published quantitative kinetic models. *BMC Syst Biol* **4**, 92.
9 Olivier B & Snoep J (2004) Web-based kinetic modelling using JWS Online. *Bioinformatics* **20**, 2143–2144.
10 Zhou M, Cheng T & Chan KCC (2010) DOCQS: a prototype system for supporting data-oriented content query. In *Proceedings of the 2010 International Conference on Management of data* (Elmagarmid AK & Agrawal D ed.), pp. 1211–1214. ACM New York, NY, USA.
11 Miller A, Marsh J, Reeve A, Garny A, Britten R, Halstead M, Cooper J, Nickerson DP & Nielsen PF (2010) An overview of the CellML API and its implementation. *BMC Bioinformatics* **8**, 178.
12 Wolstencroft K, Owen S, du Preez F, Krebs O, Mueller W, Goble C & Snoep JL (2011) The SEEK: a platform for sharing data and models in systems biology. *Methods Enzymol* **500**, 629–655.
13 Teusink B, Passarge J, Reijenga CA, Esgalhado E, Van der Weijden CC, Schepper M, Walsh MC, Bakker BM, van Dam K, Westerhoff HV *et al.* (2000) Can yeast glycolysis be understood in terms of *in vitro* kinetics of the constituent enzymes? Testing biochemistry. *Eur J Biochem* **267**, 5313–5329.
14 Pritchard L & Kell D (2002) Schemes of flux control in a model of *Saccharomyces cerevisiae* glycolysis. *Eur J Biochem* **269**, 3894–3904.
15 Bruck J, Liebermeister W & Klipp E (2008) Exploring the effect of variable enzyme concentrations in a kinetic model of yeast glycolysis. *Genome Informatics* **20**, 1–14.
16 Albers E, Larsson C, Andlid T, Walsh MC & Gustafsson L (2007) Effect of nutrient starvation on the cellular composition and metabolic capacity of *Saccharomyces cerevisiae*. *Appl Environ Microbiol* **73**, 4839–4848.
17 Rizzi M, Baltes M, Theobald U & Reuss M (1997) *In vivo* analysis of metabolic dynamics in *Saccharomyces cerevisiae*: II: mathematical model. *Biotechnol Bioeng* **55**, 592–608.
18 Hynne F, Danø S & Sørensen P (2001) Full-scale model of glycolysis in *Saccharomyces cerevisiae*. *Biophys Chem* **94**, 121–163.
19 Bier M, Bakker BM & Westerhoff HV (2000) How yeast cells synchronize their glycolytic oscillations: a perturbation analytic treatment. *Biophys J* **78**, 1087–1093.

20 Cronwright GR, Rohwer JM & Prior BA (2002) Metabolic control analysis of glycerol synthesis in *Saccharomyces cerevisiae*. *Appl Environ Microbiol* **68**, 4448–4456.
21 Galazzo J & Bailey J (1990) Fermentation pathway kinetics and metabolic flux control in suspended and immobilized *Saccharomyces cerevisiae*. *Enzyme Microb Technol* **12**, 162–172.
22 Nielsen K, Sørensen PG, Hynne F & Busse HG (1998) Sustained oscillations in glycolysis: an experimental and theoretical study of chaotic and complex periodic behavior and of quenching of simple oscillations. *Biophys Chem* **72**, 49–62.
23 Poulsen AK, Østergaard Petersen M & Olsen LF (2007) Single cell studies and simulation of cell–cell interactions using oscillating glycolysis in yeast cells. *Biophys Chem* **125**, 275–280.
24 Wolf J, Passarge J, Somsen OJ, Snoep JL, Heinrich R & Westerhoff HV (2000) Transduction of intracellular and intercellular dynamics in yeast glycolytic oscillations. *Biophys J* **78**, 1145–1153.
25 Richard P, Teusink B, Hemker MB, Dam KV & Westerhoff HV (1996) Sustained oscillations in free-energy state and hexose phosphates in yeast. *Yeast* **12**, 731–740.
26 Das J & Busse H (1991) Analysis of the dynamics of relaxation type oscillation in glycolysis of yeast extracts. *Biophys J* **60**, 369–379.
27 Ghosh A, Chance B & Pye E (1971) Metabolic coupling and synchronization of NADH oscillations in yeast cell populations. *Arch Biochem Biophys* **145**, 319–331.
28 Richard P, Bakker BM, Teusink B, Dam KV & Westerhoff HV (1996) Acetaldehyde mediates the synchronization of sustained glycolytic oscillations in populations of yeast cells. *Eur J Biochem* **235**, 238–241.
29 Boiteux A, Goldbeter A & Hess B (1975) Control of oscillating glycolysis of yeast by stochastic, periodic, and steady source of substrate: a model and experimental study. *Proc Natl Acad Sci USA* **72**, 3829–3833.
30 Goldbeter A & Lefever R (1972) Dissipative structures for an allosteric model: application to glycolytic oscillations. *Biophys J* **10**, 1302–1315.
31 Reijenga KA, van Megen YM, Kooi BW, Bakker BM, Snoep JL, van Verseveld HW & Westerhoff HV (2005) Yeast glycolytic oscillations that are not controlled by a single oscillophore: a new definition of oscillophore strength. *J Theor Biol* **232**, 385–398.
32 du Preez FB, van Niekerk DD & Snoep JL (2012) From steady-state to synchronized yeast glycolytic oscillations II: model validation. *FEBS J*, doi:10.1111/j.1742-4658.2012.08658.x.
33 Kacser H & Burns JA (1973) The control of flux. *Symp Soc Exp Biol* **27**, 65–104.
34 Heinrich R & Rapoport TA (1974) A linear steady-state treatment of enzymatic chains. General properties, control and effector strength. *Eur J Biochem* **42**, 89–95.
35 Guijarro JM & Lagunas R (1984) *Saccharomyces cerevisiae* does not accumulate ethanol against a concentration gradient. *J Bacteriol* **160**, 874–878.
36 Tehrany E & Desobry S (2005) Comparison between different calculation methods of partition coefficient of aroma compounds of different chemical classes in the octanol–water system. *Sci Aliments* **25**, 23–36.
37 Park YSPS (2000) Determination and prediction of octanol/water partition coefficients and air–water partition coefficients for environmental toxic chemicals. *J Indust Eng Chem* **11**, 773–779.
38 Wolf J & Heinrich R (2000) Effect of cellular interaction on glycolytic oscillations in yeast: a theoretical investigation. *Biochem J* **345**, 321–334.
39 De Monte S, d'Ovidio F, Danø S & Sorensen PG (2007) Dynamical quorum sensing: population density encoded in cellular dynamics. *Proc Natl Acad Sci USA* **104**, 18377–18381.
40 Ashyraliyev M, Fomekong-Nanfack Y, Kaandorp JA & Blom JG (2009) Systems biology: parameter estimation for biochemical models. *FEBS J* **276**, 886–902.
41 Cedersund G & Roll J (2009) Systems biology: model based evaluation and comparison of potential explanations for given biological data. *FEBS J* **276**, 903–922.
42 Kreutz C & Timmer J (2009) Systems biology: experimental design. *FEBS J* **276**, 923–942.
43 Rossell S, van der Weijden C, Lindenbergh A, van Tuijl A, Francke C, Bakker BM & Westerhoff HV (2006) Unravelling the complexity of flux regulation: a new method demonstrated for nutrient starvation in *Saccharomyces cerevisiae*. *Proc Natl Acad Sci USA* **103**, 2166–2171.
44 Madsen MF, Danø S & Sørensen PG (2005) On the mechanisms of glycolytic oscillations in yeast. *FEBS J* **272**, 2648–2660.

Supporting information

The following supplementary material is available:
Fig. S1. Results for the objective function for synchronization.
Table S1. Comparison of phases, amplitudes and mean concentration for the model simulations and experimental data.
Table S2. All parameter values for the models.

This supplementary material can be found in the online version of this article.

Please note: As a service to our authors and readers, this journal provides supporting information supplied by the authors. Such materials are peer-reviewed and may be reorganized for online delivery, but are not copy-edited or typeset. Technical support issues arising from supporting information (other than missing files) should be addressed to the authors.